Glycine Residue Twists HOMO...HOMO Interactions in a Molecular Conductor

Abdelkrim El-Ghayoury, Cecile Meziere, Sergey Simonov, Leokadiya Zorina, Pascale Auban-Senzier, Pere Alemany, Enric Canadell, Patrick Batail

Glycine Residue Twists HOMO···HOMO Interactions in a Molecular Conductor

Abdelkrim El-Ghayoury[*,a] Cécile Mézière,[a] Sergey Simonov,[b] Leokadiya Zorina,[b] Pascale Auban-Senzier,[c] Pere Alemany,[d] Enric Canadell,*[,e] and Patrick Batail*[,a]*

[a] *Laboratoire MOLTECH-Anjou, UMR 6200, CNRS, Université d'Angers, France*

[b] *Institute of Solid State Physics, Russian Academy of Sciences, Chernogolovka MD, Russia*

[c] CNRS, *Laboratoir e de Physique des Solides, Université Paris-Saclay, 91405 Orsay, France*

[d] *Departament de Ciència de Materials i Química Física and Institut de Química Teòrica i Computacional (IQTCUB), Universitat de Barcelona, Martí i Franques 1, Barcelona 08028, Spain*

[e] *Institut de Ciència de Materials de Barcelona (ICMAB-CSIC), Campus de la UAB, 08193 Bellaterra, Spain*

Abstract

We report on radical cation salts of EDT-TTF cores bearing a glycine residue with hydrogenosulfate, [HSO_4^-] or the amphoteric *para*-carboxybenzenesulfonate, [HO_2C-C_6H_4-SO_3^-]. In (EDT-TTF-CO-$NHCH_2$-CO_2H)$_2^+$[HSO_4^-], orthogonal pairs of oxygen atoms of the tetrahedral sulfonate anions engage in hydrogen bonds building the 2D chess-board pattern of orthogonal dimers typical of a κ-phase 2D metal. We find by tight-binding and DFT analysis of the band structure that as a result of the structure-directing role of the gly residue, HOMO···HOMO interactions in (EDT-TTF-CO-$NHCH_2$-CO_2H)$_2^+$[HSO_4^-] are twisted away from the usual in-plane isotropy of κ-phases towards a very uncommon quasi-1D electronic structure with electronic localization. Transport measurements confirm the highly conducting, yet weakly localized regime. The ability of *para*-carboxybenzenesulfonate to act as a bi-molecular, dianionic unit of double spatial extension is fulfilled in (EDT-TTF-CO-$NHCH_2$-CO_2H)$_2^{2+}$[HO_2C–C_6H_4–SO_3^-]$_2$ where the charge is balanced by diamagnetic dimers leaving no carrier left available in the lattice.

INTRODUCTION

The past decades have witnessed the growth of $TTF^{\bullet+}$ radical cation chemistry[1] and the rise of TTF science, encompassing a large physics component, whose milestones include the discovery of organic metals, organic superconductors, and organic solar cells.[2,3] Balancing π-overlap and intermolecular hydrogen-bonding interactions[4-7] to affect the collective electronic properties of organic conductors has been a key design principle of materials that include bi-component charge-transfer complexes, radical cation salts, and the emerging class of proton-doped single-component crystalline systems.[8]

TTF derivatives appended with hydrogen-bond donor/acceptor functionalities include alcohols such as $Me_3TTF(CHMeOH)$;[9] $TTF(CH_2OH)_4$;[10] EDT-TTF-$(CH_2OH)_n$[11,14] thioamides;[15] mono- and diamides; uracil-derivatized TTFs;[16] adenine-derivatized TTF;[17-20] and the anilinium phosphonate $PhNH_3^+Me_3TTF\text{-}PO_3H^-$ and its zwitterionic form, $[Me_3TTF\text{-}PO_3H^-]^+$.[12] Note that organic metals have been designed using intermolecular hydrogen bonding interactions as in the radical cation salt β''-$(EDT\text{-}TTF\text{-}CONHMe)_2[Cl{\cdot}H_2O]$[6], the charge transfer complex TTF-imidazole-p-chloranil,[13] as well as in the case of single-component metals based on catechol-fused tetrathiafulvalenes.[21-22]

In the wake of this research, we recently focussed on (EDT-TTF-CO-$NHCH_2$-CO_2H), **1** (Scheme 1), seeing its ethylenedithiotetrathiafulvalene core appended with a glycine ionizable residue as a dormant, redox-active π-conjugated zwitterion to be activated by coupled charge transfer and acid/base reactions. As it turned out, the outcome is not the self-assembled single-component zwitterionic solid **2** but a bi-component **1**:**2** adduct instead, achieving a fine balance of chemical potentials in a pair of acidic and basic neutral partners.[23]

Scheme 1

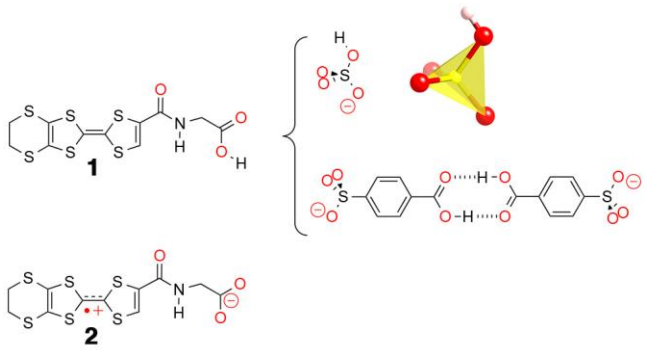

Seeking to explore the hydrogen-bonding donor/acceptor ability of a glycine residue appended to a TTF core we report in this study on the deliberate association of radical cation $\mathbf{1}^+$ with either the hydrogenosulfate, $[HSO_4^-]$ or the amphoteric *para*-carboxybenzenesulfonate, $[HO_2C\text{-}C_6H_4\text{-}SO_3^-]$ anions (Scheme 1), adding with the latter another degree of complexity because of it may act either as a discrete, single anion or as a bi-molecular, dianionic unit of

double spatial extension on account of the stabilization of typical self-complementary carboxylic acid hydrogen bonded dimers.

RESULTS AND DISCUSSION

κ-(1)$_2^+$[HSO_4^-]

As shown in Figure 1, single layers of radical cations and hydrogenosulfate anions alternate along *c*. The triclinic unit cell includes two independent EDT-TTF-$CONHCH_2CO_2H$ molecules self-assembled into mixed-valence dimers I (A-A) and II (B-B) whose central C=C double bond lengths amount to 1.361(4) and 1.368(4) Å in A and B, respectively. Both molecules are planar as they fold about S-S lines between central and outer parts of EDT-TTF fragment by less than 3° while the same angles are of typically 5° in neutral molecules. The outer ethylene group of molecule B is disordered between two positions with 0.55/0.45 occupancies. The -COOH group is not coplanar with the π-conjugated cores: torsion angles about N-C bond of C-N-C-C fragments are 103.4(3)° and 82.7(3)° in A and B, respectively (102.4° in neutral molecule).[23]

The strongest hydrogen bond donors capture the three oxygen atoms of each anion (interactions 1-4 in Table 1), effectively relaying the orientation of orthogonal pairs of oxygen atoms of the tetrahedral sulfonate anions so that A and B are orthogonal (Figure 1b). This motif extends further into a layered structure with the typical chessboard pattern of a κ-type topology (Figures 1 and 2). Adjacent strong N-H···O and C_{sp2}-H···O hydrogen bonds of B cooperate in a tweezers-like motif to grab the fourth oxygen atom of the anion (interactions 6, 7 in Figs. 1b-c and Table 1). The acid oxygen atom of B is captured by a similar pair out of A (4 and 5, Figure 1c). Note that in the monocomponent crystals of **1**, pairs of O-H···O bonds between acid groups connect two molecules into dimers,[24] and tweezers-like motifs lock adjacent –NH and $-C_{sp2}H$ donors of one molecule on the carbonyl oxygen atom of another one. Both motifs do not exist in the structure of (**1**)$_2^+$[HSO_4^-]; here, the carboxylic acids of both A and B react with the anion and carbonyl O is not involved into any tweezers-type hydrogen bonding. In addition, oxygen atoms of the carbonyl C=O groups of the donor are involved in lateral S···O interactions with neighboring TTF (3.04 and 3.02Å) shorter than in (**1**)$_2^{2+}$[$HO_2C–C_6H_4–SO_3^-$]$_2$ (S···O distances 3.195(2),3.232(2) and 3.236(3) Å).

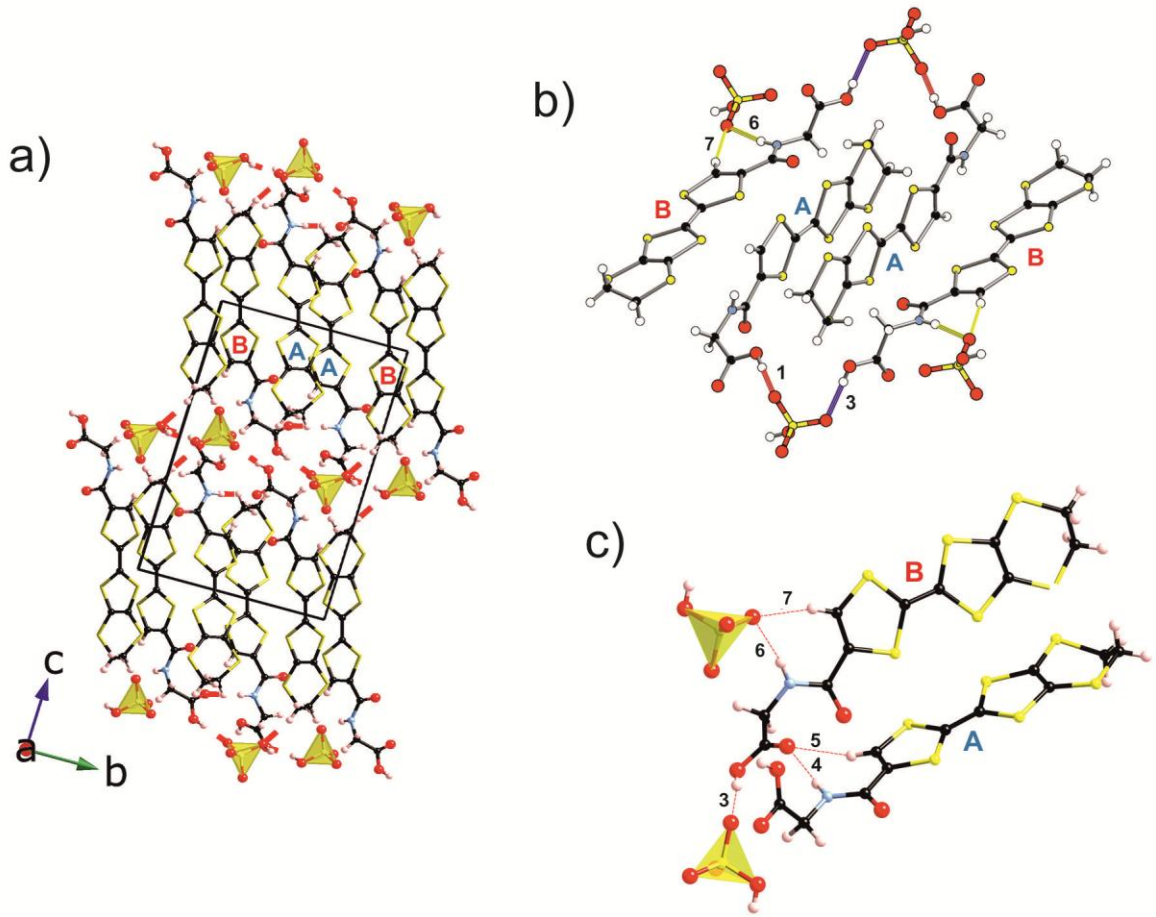

Figure 1. a) Layered structure of $[\mathbf{1}]_2^+[HSO_4^-]$. b) and c) Fragments of the hydrogen network (Table 1) primarily involved in directing the quasi-orthogonality between A and B, thereby developing onto the κ-type topology shown in Figure 2.

Table 1. Hydrogen-bonding in κ-$[\mathbf{1}]_2^+[HSO_4^-]$ and $(\mathbf{1})_2^{2+}[HO_2C–C_6H_4–SO_3^-]_2$

Interaction	Contact type	Molecules	H···A, Å	D···A, Å	D-H-A, °
κ-$[\mathbf{1}]_2^+[HSO_4^-]$					
1	O_{acid}-H···O_{anion}	A···anion	1.90	2.714(3)	172.4
2	O_{anion}-H···O_{acid}	anion···A	1.80	2.561(4)	153.0
3	O_{acid}-H···O_{anion}	B···anion	1.86	2.619(3)	172.8
4	N-H···O_{acid}	A···B	2.30	3.157(3)	177.4
5	C_{cp2}-H···O_{acid}	A···B	2.27	3.135(4)	154.9
6	N-H···O_{anion}	B···anion	2.09	2.942(3)	170.6
7	C_{cp2}-H···O_{anion}	B···anion	2.35	3.250(4)	162.8
$(\mathbf{1})_2^{2+}[HO_2C–C_6H_4–SO_3^-]_2$					

1	O_{acid}-H···O_{acid}	anion···anion	1.82	2.633(3)	169.0
2	O_{acid}-H···O_{SO3}	donor···anion	1.92	2.658(3)	148.5
3	N-H···O_{SO3}	donor···anion	2.08	2.929(3)	167.3
4	C_{cp2}-H···O_{SO3}	donor···anion	2.39	3.283(3)	159.9

The chessboard pattern of association of dimers I (A-A) and II (B-B) (Fig. 2) is typical of a κ-type topology. The dihedral angle between A and B is 72.17(2)°. Intradimer separations between planes of the six atoms of TTF-cores are 3.51(3) in dimer I (Fig. 3a) and 3.47(1) Å in II (Fig. 3b) with identical ring-over-bond mode of overlap. Note that the acid groups are directed toward the centre of dimer I, and point outside dimer II, so that S···S contacts are shorter in II while exceeding the sum of van der Waals radii, 3.7 Å (Table 2) in I.

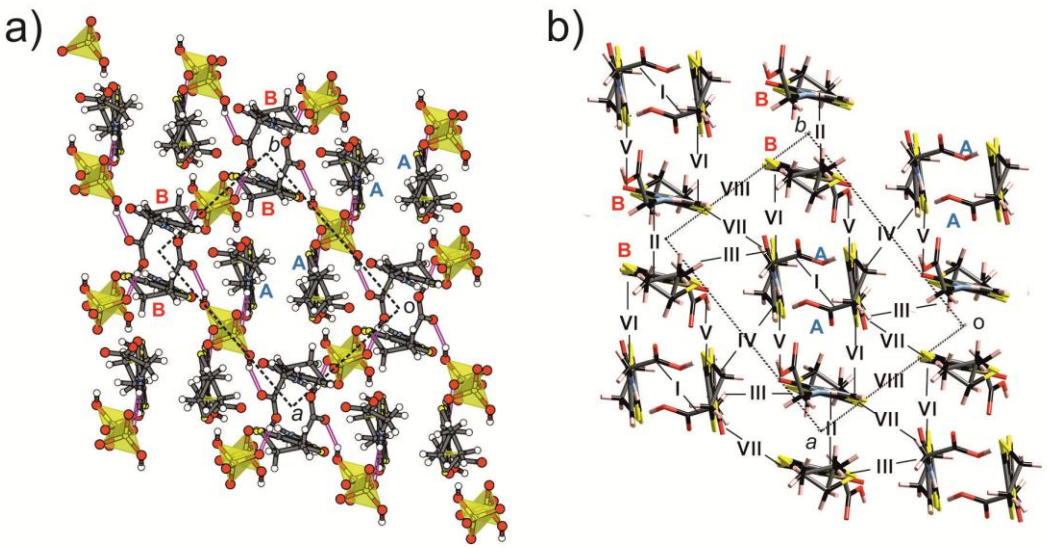

Figure 2. Bird-eye view of a single *ab* layer of Figure 1a showing the chessboard pattern of association of mixed-valence dimers in κ-[**1**]$_2^+$[HSO_4^-]: a) Location of anions (in yellow) above and below the donor layers, and b) Distribution of different intermolecular interactions I to VIII between molecules A and B.

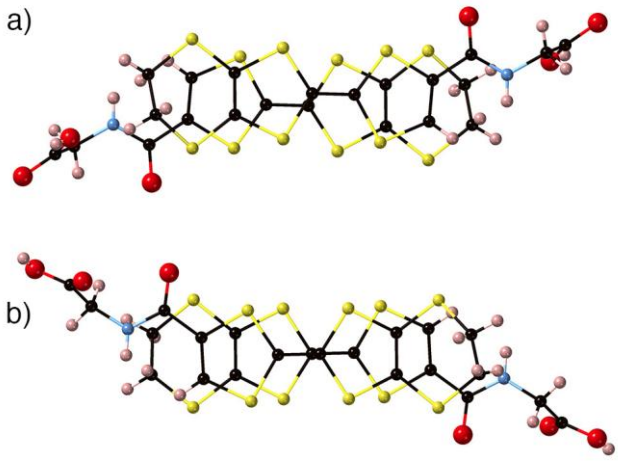

Figure 3. (a) Intradimer interactions for a) dimer I; and b) dimer II.

The donor layers of κ-(**1**)$_2^+$[HSO_4^-] contain two different donor molecules with eight different intermolecular interactions between them (noted I to VIII in Fig. 2b). The distances for S···S contacts and the absolute values of the HOMO···HOMO intermolecular interaction energy,[25] $|\beta_{HOMO\text{-}HOMO}|$, associated with any of these interactions are reported in Table 2. The $\beta_{HOMO\text{-}HOMO}$ values are a measure of the strength of the interaction between a pair of donor HOMOs in adjacent sites of the crystal. Since it is the HOMO levels which are at the origin of the transport properties of molecular conductors, these interaction energies have been extremely valuable in correlating the structure and properties of molecular conductors.[26] The calculated band structure and Fermi surface for the donor layers of [**1**]$_2^+$[HSO_4^-] are shown in Figure 4. The band structure is quite different from those typical for κ-phases.[27] Whereas there is a clear dispersion along *a**, this is not the case along *b**. This is suggestive of a one-dimensional system and it is confirmed by the calculated Fermi surface (see Fig. 4b): a textbook example of a 1D system along *a*.

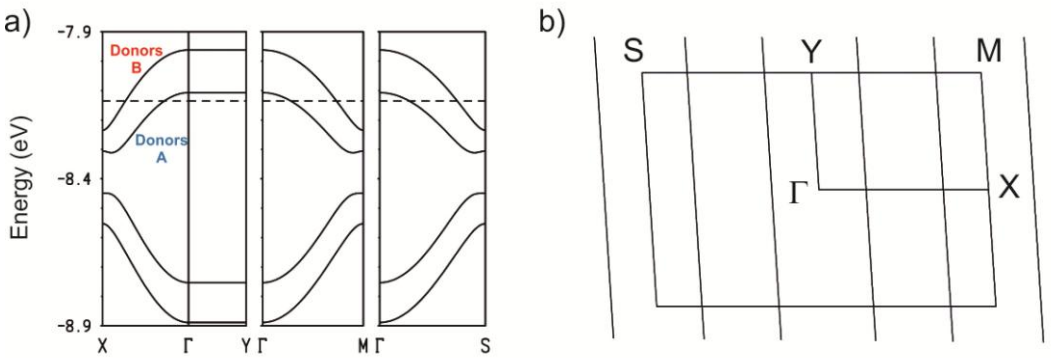

Figure 4. Extended Hückel band structure (a) and Fermi surface (b) for a donor layer in κ-(**1**)$_2^+$[HSO_4^-]. The dashed line refers to the Fermi level and Γ = (0, 0), X = (*a**/2, 0), Y = (0, *b**/2), M = (*a**/2, *b**/2) and S = (-*a**/2, *b**/2).

As discussed before, the donor layers contain two different donors A and B. From the viewpoint of their HOMOs both donors are very similar, -8.578 eV (A) and -8.554 eV (B). In contrast, dimers A-A and B-B are very different because of the different overlap induced by the substituents. As shown in Table 2, interaction B-B (II) within the dimer is considerably stronger than interaction A-A (I). The antibonding combination of the HOMOs in dimer B-B is higher in energy than that in dimer A-A essentially because in the first the S···S contacts are shorter. This is why the upper band in Figure 4a is mainly built from the HOMOs of donor B whereas the next one is mostly built from those of donor A. There are two electrons to fill these 1D bands and since they overlap, both are partially filled. Thus the system could be a 1D metal along *a*. To understand the unexpected 1D character of the system we must look at the different HOMO···HOMO interactions. As for any κ-phase, the layers are built from two series of dimers along one of the two principal directions (in this case *a*). Dimers A-A are coupled along *a* through interaction IV and dimers B-B interact thought interaction VIII. The coupling between the two different chains occurs via A-B interactions (III, V, VI and VII). Depending on the relative strength of interdimer A-A and B-B interactions along *a*, and the A-B interactions coupling the dimer chains, the system may be 1D or 2D. Both intrachain interactions (IV and VIII) are strong whereas all the interchain interactions are weak except for VII which is of medium strength. Consequently, from the viewpoint of the HOMO···HOMO interactions the system may be described as a series of weakly interacting chains of dimers along *a*. Looking at the different intermolecular interactions it is clear that the presence of the substituent does not allow for a good overlap for interactions III, V and VI while it makes interaction A-A (I) weaker than B-B (II). In fact, these observations are directly related to the hydrogen-bonding pattern of interactions with the anions discussed in the preceding section. The anions sit directly above and below interactions IV and VIII (see Figure 2b) imposing the unusually strong HOMO···HOMO interactions along dimers in the *a*-direction and thus, being ultimately responsible for the unusual 1D electronic structure of this salt.

Table 2. S···S distances and associated $|\beta_{HOMO\text{-}HOMO}|$ energies for the different intermolecular interactions in the donor layer of κ-(**1**)$_2^+$[HSO_4^-].

Interaction	S···S (<4.0Å)	$\lvert\beta_{HOMO\text{-}HOMO}\rvert$ (eV)

I	(A-A)	3.731, 3.821(x2), 3.867(x2), 3.929(x2)	0.2924
II	(B-B)	3.650(x2), 3.662(x2), 3.823(x2), 3.989(x2)	0.4441
III	(A-B)	3.920	0.0593
IV	(A-A)	3.628(x2)	0.2797
V	(A-B)	3.480, 3.490, 3.585, 3.698, 3.901	0.0252
VI	(A-B)	3.893	0.0498
VII	(A-B)	3.635, 3.691, 3.855, 3.995	0.1362
VIII	(B-B)	3.654(x2), 3.773(x2)	0.2395

The results in Figure 4, based on one-electron band theory, can be compatible with two different physical situations depending on the strength of electronic repulsions. If they are weak, double occupation of the levels would lead to a one-dimensional (1D) metal. In contrast, if electron repulsions are strong enough, the system would become a localized 1D semiconductor with one hole located on each dimer. In the present case, the two possibilities can be in principle distinguished by looking at the charge distribution. According to the results of Figures 4, a metallic description of the system would lead to an important charge difference between donors A and B (i.e. approximately +1/4 for A and +3/4 per B) and thus on the HOMOs and central C=C distances. This is not quite consistent with the observed small difference between the two HOMOs (see above) as well as between the two central C=C distances (1.361 Å for A and 1.368 Å for B) so that a localized 1D system seems more likely.

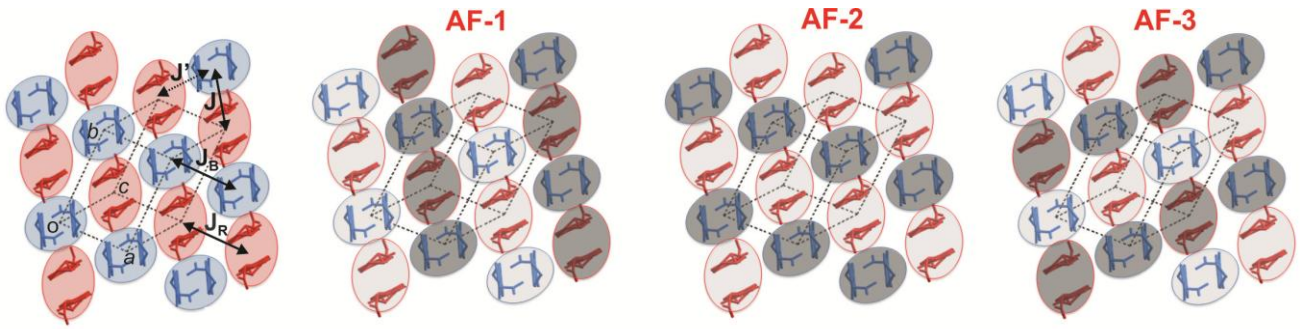

Figure 5. (a) Geometry of a single layer of κ-(**1**)$_2^+$[HSO_4^-] highlighting the two different types of dimers in blue(A)/red(B) colour. The different exchange interactions between dimers are noted. (b)-(d) Three different antiferromagnetic states where the shaded dimers are associated with spin up and the non-shaded dimers with spin down.

To elucidate this point, we have carried out first-principles density functional theory (DFT) calculations for the metallic system and several localized configurations of the κ-(**1**)$_2^+$[HSO_4^-] salt, i.e. ferromagnetic (FM) and the three antiferromagnetic (AF1, AF2 and AF3) states of Figure 5. These AF states are all the antiferromagnetic states that can be built from a cell twice larger than the crystallographic cell (i.e. *a*'= 2*a, b*'= *b* and *c*'=*c*). In these states there are chains of dimers making ferromagnetic interactions along one of the directions *a*, (*a*+*b*) or (*a*-*b*) and antiferromagnetic interactions along the other two. The metallic state was found to be higher in energy than all localized states: Metallic (+1192 K), Ferromagnetic (0 K), AF-1 (-9.4 K), AF-2 (+0.2 meV) and AF-3 (-9.4 K). Note that the AF-1 and AF-3 have the same energy although they are not strictly equivalent by symmetry. The DFT band structures for the metallic, ferromagnetic and the antiferromagnetic AF-1 states are shown in Figure 6. The band structure of the AF-3 (Figure S2b) is undistinguishable from that for AF-1. These band structures have all been calculated with the above-mentioned double cell to facilitate the comparison with the more stable AF-1 and AF-3 states. The band structure of the metallic state (Figure 6a) is very similar to the Extended Hückel one, although they may look different because of the use of a double cell. Since the cell parameter along *a* has been doubled, the bands along Γ-X in Figure 6a must be unfold (i.e. the total dispersion along the *a*-direction is given by the energy difference at Γ of the two bands degenerate at X, see Figure S1). The only difference is a weak dispersion in the interlayer direction Γ-Y so that the metallic system would really be pseudo-1D.

The effect of the electronic repulsions is clearly seen for the FM state shown in Figure 6b where the spin up (red) and spin down (blue) bands are almost rigidly shifted and have the same shape as in the metallic state. However, in the metallic state the occupation of the two upper bands was very different, resulting with chains of electron-rich and electron poor dimers. In the ferromagnetic state the occupation of the two types of bands is the same so that all dimers have the same charge and this result in a clear stabilization. We conclude thus that charge separation is disfavoured by the electronic repulsions. Using the four different exchange interactions noted in Figure 5a the energies of the four magnetic states considered are: FM= 0, AF-1= $2(J_B+J_R)+ 4J'$, AF-2= $4(J+J')$ and AF-3= $2(J_B+J_R)+ 4J$. Taking into account the calculated energies we obtain $J = J' \approx$ +0.5 K which are clearly smaller than J_B and J_R for which we found that $J_B+J_R \approx$ -5 K (larger unit cells would be needed to separate them). In other words, the system prefers to have antiferromagnetic interactions along the chains with the same colour, which is precisely what happens in states AF-1 and AF-3. As a result of the antiferromagnetic interactions along *a,* the dimers are engaged in ferromagnetic interactions along either the (*a*+*b*) or (*a*-*b*) directions and antiferromagnetic interactions along the other. The states AF-1 and AF-3 correspond to the two possibilities. The difference in the interdimer interactions along these directions is too small to

definitely favour one of the two. The band structure for AF-1 is shown in Figure 6c where a larger band gap occurs because of the antiferromagnetic interaction along the blue/red chains. Every band in this figure is really a pair of identical bands, one associated with spin up and the other with spin down. The two upper, empty ones corresponding to the holes are mostly centered on the red B dimers (upper) and the blue A dimers (lower) as expected for a system with weak antiferromagnetic interactions along *a*. Note however that the energy differences between the different localized states is quite small, so that we do not expect that the antiferromagnetic ordering can occur except maybe at very low temperatures. We thus conclude that the occurrence of dimers with very similar donors but different intra-dimer HOMO···HOMO interaction in this salt is only compatible with a non-ordered localization of holes within the dimers.

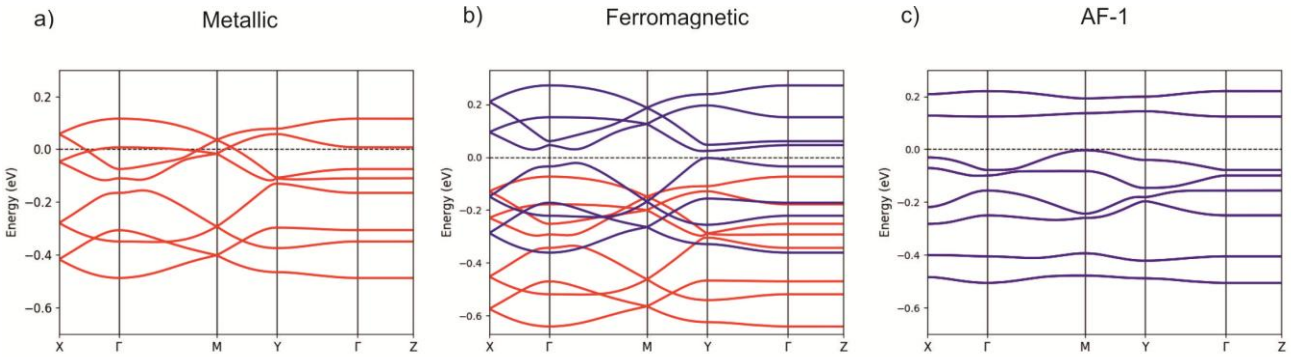

Figure 6. DFT band structures for the metallic (a), ferromagnetic (b) and antiferromagnetic AF-1 states of κ-(**1**)$_2^+$[HSO_4^-] calculated using a double cell (*a*'= 2*a*, *b*'= *b* and *c*'= *c*). Γ = (0, 0, 0), Y = (0, *b*'*/2, 0), Z = (0, 0, *c*'*/2), M = (0, *b*'*/2, *c*'*/2) and X (*a*'*/2, 0, 0). The dashed line refers to the highest occupied level in all cases. All levels are doubly filled in (a). Spin up and spin-down bands are shown in red and blue, respectively in (b) and (c). The spin-up and spin-down bands are identical although located in spatially different but equivalent sites in (c) so that only the blue bands are visible.

Room temperature, in-plane and inter-plane conductivities are $\sigma_{//}$ = 5 S/cm and $\sigma_{\perp}$ = 3.6 10^{-4} S/cm, respectively, which gives an anisotropy ratio $\sigma_{//} / \sigma_{\perp} = 10^4$. While this value is typical for 1D molecular conductors such as $(TMTTF)_2X$ or $(TMTSF)_2X$,[28] it is much larger than for other κ-phases of BEDT-TTF salts (between 25 and 100),[29,30] which in contrast with the present salt have quite isotropic HOMO···HOMO interactions within the donor plane. Considering the in-plane resistivity, a weak localization is observed when cooling down to 100 K, then an activated regime

sets in with $E_{act//}$ = 500 K (see Fig. 7) which can be associated with a Mott insulating state (the Mott gap is defined by $\Delta = 2\ E_{act//}$). The temperature dependence of the out-of-plane resistivity shows a localization associated with a small activation energy $E_{act\perp}$ = 250 K (which is of the order of the temperature) despite a high resistivity value. This suggests that, as for κ-phases of BEDT-TTF salts, the out-of-plane resistivity mimics the in-plane resistivity. However, the change of regime around 100 K (at the onset of Mott insulating state) is not clearly visible.

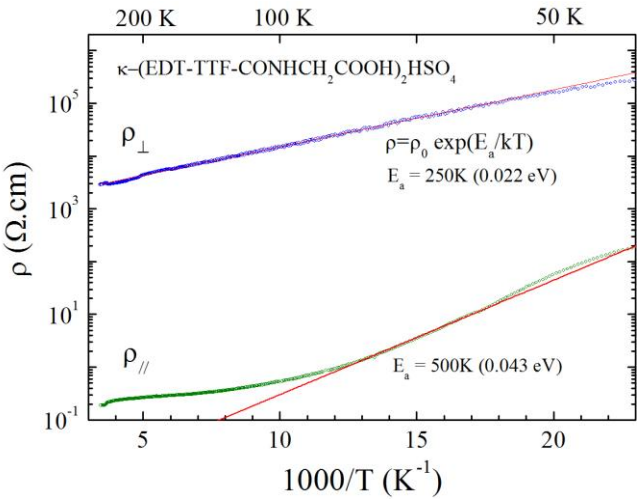

Figure 7. Variable-temperature in-plane ($\rho_{//}$) and out-of-plane ($\rho_{\perp}$) resistivities for κ-(**1**)$_2^+$[HSO_4^-] plotted as log (ρ) versus 1/T. Solid lines are the fit of the data to $\rho = \rho_0 \exp(E_a/T)$, qualifying the activated regime.

(1)$_2^{2+}$[$HO_2C–C_6H_4–SO_3^-$]$_2$: strong diamagnetic dimers, no carriers

As shown in Figure 8, in this case the two strongest hydrogen-bond donors capture the two best hydrogen-bond acceptors to form interactions 2 and 3. Hence, typical hydrogen-bonded carboxylic acid dimers (Scheme 1) are stabilized unperturbed despite their O–H···O hydrogen bond being notably weaker. Strongly dimerized pairs of radical cations achieve charge balance. The monoclinic unit cell with $P2_1/n$ symmetry contains one independent EDT-TTF-$CONHCH_2COOH$ and one *p*-carboxybenzenesulfonate anion in general position. The outer ethylene group of EDT-TTF fragment is disordered between two sites with 0.60/0.40 occupancies. The TTF core mean planes and the anion within the same layer make a dihedral angle of 18.17(8)°. An elongated central C=C bond in the TTF-core with bond distance of 1.398(3) Å indicates a fully charged state (+1) for **1**. Near direct overlap of TTF fragments in dimeric units is associated with very short S···S contacts (3.441(1) Å (×2) and 3.474(1) Å (×2))

whereas the interdimer lateral interaction occurs via two pairs of identical S···S contacts at 3.761(1) Å and 3.934(1) Å.

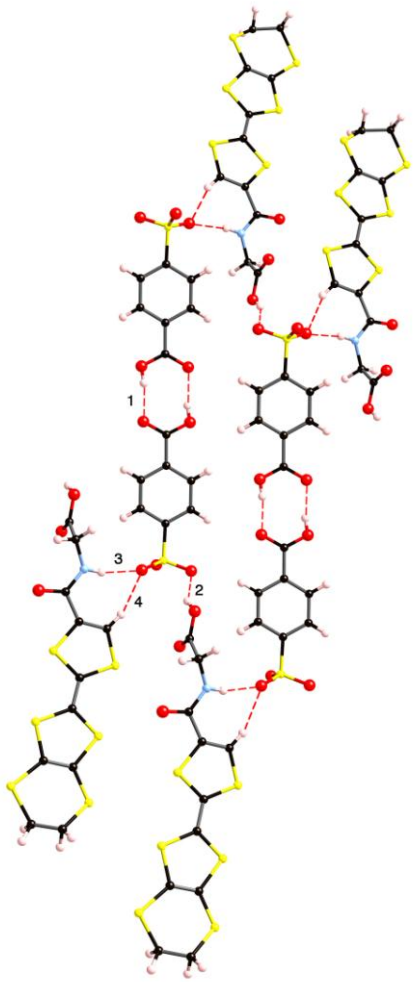

Figure 8. Pattern of hydrogen-bonding interactions in $(\mathbf{1})_2^{2+}[HO_2C–C_6H_4–SO_3^-]_2$. Bonds labels refer to Table 1.

As for $(\mathbf{1})_2^{+}[HSO_4^-]$, an extensive network of hydrogen bonds is identified in the structure of $(\mathbf{1})_2^{2+}[HO_2C–C_6H_4–SO_3^-]_2$ (Figure 8 and Table 1). There is a clear bond length difference between the C=O double bond, 1.193(4) Å, and the C-O(H) single bond, 1.308(3) Å in the –COOH moiety of $\mathbf{1}^+$ whereas in the anion similar bond distances are closer to each other, 1.254(3) and 1.265(3) Å, respectively. Although in the latter case the hydrogen atom may eventually be disordered between both oxygen atoms of the acid, the difference electron density map shows only one preferable position for H. The tweezer-like hydrogen bonds 3 and 4 capture the oxygen atoms of the anion whereas the oxygen atoms of two carbonyl C=O groups of the donor are only involved in lateral S···O interactions between donors from adjacent dimers, with S···O distances 3.195(2), 3.232(2) and 3.236(3) Å. Therefore, in keeping with a recurrent observation,[4] it is also apparent

in the structure of $(\mathbf{1})_2^{2+}[HO_2C–C_6H_4–SO_3^-]_2$ that the hydrogen bond acceptor ability of carbonyl oxygen of the amide group-appended TTF-core is de-activated in the radical cation.

The calculated $|\beta_{HOMO\text{-}HOMO}|$ values for two donors in the same and adjacent dimers are 0.8159 eV and 0.0003 eV, respectively, qualifying a very strong interaction within the dimers while the interaction between dimers is practically nil so that these donor chains are simply chains of non-interacting, doubly charged strong dimers. Accordingly, the calculated extended Hückel band structure for the full layer (Figure S3) exhibits a large band gap of 0.87 eV separating very flat bands associated with the bonding and antibonding levels of the dimers and the system should be an intrinsic band gap insulator.

CONCLUSION

The hydrogen-bonding donor/acceptor ability of a glycine residue appended to a TTF core is fully exercised, forming tweezers-like motifs that capture orthogonal pairs of oxygen atoms of the tetrahedral sulfonate anions in two new molecular conductors. In $(EDT\text{-}TTF\text{-}CO\text{-}NHCH_2\text{-}CO_2H)_2^+[HSO_4^-]$ the π-conjugated planar radical cations are directed to form an angle of 72°, ultimately imposing the extended lattice to adopt the typical 2D topology of a κ-phase. Surprisingly, the resulting phase is not a 2D metal, but a highly conducting albeit slightly localized 1D electronic system instead. Despite the inherent complexity of the hydrogen bonding interactions brought about by deliberate use of a glycine residue, DFT calculations reveal that control of the intermolecular interaction ensues. The HOMO···HOMO interactions are twisted away from the usual in-plane isotropy of the κ-phases towards a very uncommon quasi-1D electronic structure. Likewise, the ability of *para*-carboxybenzenesulfonate to act as a bi-molecular, dianionic unit of double spatial extension on account of the stabilization of typical, self-complementary carboxylic acid hydrogen bonded dimers is fulfilled in $(EDT\text{-}TTF\text{-}CO\text{-}NHCH_2\text{-}CO_2H)_2^{2+}[HO_2C–C_6H_4–SO_3^-]_2$. As a result, the charge is balanced by strong diamagnetic dimers leaving no carrier left available in the lattice.

EXPERIMENTAL SECTION

Synthesis of single crystals of $(\mathbf{1})_2^+[HSO_4^-]$ and $(\mathbf{1})_2^{2+}[HO_2C–C_6H_4–SO_3^-]_2$

$EDT\text{-}TTF\text{-}CO\text{-}NHCH_2\text{-}CO_2H$ was prepared as described previously.[31] [18-crown-6] and $KO_3SC_6H_4CO_2H$ were purchased from Acros and Avocado, respectively. Single crystals of $(\mathbf{1})_2^+[HSO_4^-]$ were grown at room temperature on a platinum wire electrode by galvanostatic oxidation (1 μA) of a tetrahydrofuran/acetonitrile (50:50, 12 mL) solution of **1** in the presence of

tetrabutylammonium hydrogenosulfate. $(\mathbf{1})_2^{2+}[HO_2C–C_6H_4–SO_3^-]_2$ was similarly prepared using a dichloromethane/methanol (50:50, 12 mL) solution of **1** and potassium *p*-carboxybenzenesulfonate and [18-crown-6]. Typical amounts of reactants and reaction times for the preparation of $(\mathbf{1})_2^+[HSO_4^-]$: 5 mg of **1**: 45 mg of $TBAHSO_4$; 15 days and for $(\mathbf{1})_2^{2+}[HO_2C–C_6H_4–SO_3^-]_2$: donor molecule 5 mg of **1**; 65 mg of [18-crown-6] ; 50 mg of $KO_3SC_6H_4CO_2H$; 15 days.

X-ray diffraction

X-ray diffraction data of single crystals of $(\mathbf{1})_2^+[HSO_4^-]$ and $(\mathbf{1})_2^{2+}[HO_2C–C_6H_4–SO_3^-]_2$ were collected at room temperature using a Bruker Nonius KappaCCD diffractometer with MoK_α-radiation (λ = 0.71073Å, graphite monochromator). The combined φ- and ω-scan method was used for data collection. Empirical absorption correction of experimental intensities was applied for all data. The structures were solved by a direct method followed by Fourier syntheses and refined by a full-matrix least-squares method using the SHELX-97 programs.[31] All non-hydrogen atoms in these compounds were refined in an anisotropic approximation. H-atoms were placed in idealized positions and refined using a riding model. Details of experimental data collection and structure refinement are summarized in Table 3.

Table 3. Crystal data, data collection and refinement details

	$(\mathbf{1})_2^+[HSO_4^-]$	$(\mathbf{1})_2^{2+}[HO_2C–C_6H_4–SO_3^-]_2$
Temperature	295 K	295 K
Chemical formula	$C_{22}H_{19}N_2O_{10}S_{13}$	$C_{18}H_{14}NO_8S_7$
Formula weight	888.17	596.72
Crystal system	Triclinic	Monoclinic
a, Å	8.0689(4)	7.783(1)
b, Å	11.739(2)	10.903(1)
c, Å	17.371(2)	26.977(2)
α, °	87.30(1)	90
β, °	79.746(8)	94.547(9)
γ, °	86.359(9)	90
V, Å^3	1614.8 (3)	2282.0(5)
Space group, Z	P -1, 2	$P2_1/n$, 4
$\rho_{calc.}$, g/cm^3	1.827	1.737
μ, cm^{-1}	9.35	7.40
F (000)	906	1220
Θ range, °	2.07 - 27.50	3.65 - 27.56
Index ranges	-10≤h≤10 -15≤k≤15 -22≤l≤22	-10≤h≤8 -14≤k≤12 -35≤l≤35
Reflections collected	31408	34489
Independent reflections	7372	5229
R_{int}	0.0456	0.0537

No. of variables	438	328
GooF on F^2	1.016	1.000
Final R [$I > 2\sigma(I)$]	0.0433	0.0425
CCDC	1429187	1429188

Band structure calculations

The tight-binding band structure calculations[33] were of the extended Hückel type. A modified Wolfsberg-Helmholtz formula was used to calculate the non-diagonal $H_{\mu\nu}$ values.[34] All valence electrons were taken into account in the calculations and the basis set consisted of Slater-type orbitals of double-ζ quality for C, N and O 2s and 2p, S 3s and 3p and of single-ζ quality for H. The ionization potentials, contraction coefficients and exponents were taken from previous work.[35-36]

The first-principles both spin-polarized and non-spin-polarized calculations were carried out using a numeric atomic orbitals density functional theory (DFT) approach[37,38] developed for efficient calculations in large systems and implemented in SIESTA code.[39-41] We used the generalized gradient approximation (GGA) to DFT and, in particular, the functional of Perdew, Burke, and Ernzerhof.[42] Only the valence electrons are considered in the calculation, with the core being replaced by norm-conserving scalar relativistic pseudopotentials[43] factorized in the Kleinman–Bylander form.[44] We have used a split-valence double-ζ basis set including polarization orbitals with an energy shift of 10 meV for all atoms.[44] The energy cutoff of the real space integration mesh was 300 Ry. As in recent work[46] concerning molecular conductors we have used an effective Hubbard correction term (U)[47] for S 3p orbitals of 6 eV. The Brillouin zone was sampled using a grid of (9×9×3) *k*-points for calculations using a single cell and (5×9×3) *k*-points for calculations using a double cell.[48] The crystal structure at room temperature was used for the calculations.

Transport measurements

As usual for κ-phases, single crystals of $(\mathbf{1})_2^+[HSO_4^-]$ are platelets with a rectangular face elongated along *a*. The resistivity has been measured within the plane containing layers of dimers with current flowing along *a* as well as along *c*. However, due to the small size of the crystals, it was not possible to probe resistivity along *b* so that we could not estimate the transport anisotropy in the plane. Moreover, in-plane measurements show about 20% of temperature-independent unnested voltage that can be related to either a small anisotropy in the plane or rather more likely to defects perturbing the current lines between the voltage contacts.

Gold pads were evaporated on the surface of the crystals in order to improve the quality of the contacts. Then a standard four points technique was used with a low frequency lock-in detection

(I_{ac} = 0.1-1 μA) for measured resistances below 50 kΩ and dc measurement for higher resistances (I_{dc} = 0.1-0.01 μA). Transport measurements were performed down to helium temperature.

ACKNOWLEDGMENTS

L. Z. and S. S. gratefully acknowledge support from the CNRS and the Région Pays de la Loire for an associated researcher and post-doctoral position, respectively. Financial support from the ANR PNANO Project TTF-Based Nanomat ANR-07-NANO-030-01 is gratefully acknowledged. Work in Spain was supported by MICIU (PGC2018-096955-B-C44 and PGC2018-093863-B-C22), MINECO through the Severo Ochoa (SEV-2015-0496) and Maria de Maeztu (MDM-2017-0767) Programs and the Generalitat de Catalunya (2017SGR1506 and 2017SGR1289).

ASSOCIATED CONTENTS

Supporting Information

The Supporting Information is available free of charge on the ACS Publications website at DOI: ..... Additional figures as mentioned in the text (PDF).

Accession Codes

CCDC 1429187 ((**1**)$_2^+$[HSO_4^-]) and CCDC 1429188 ((**1**)$_2^{2+}$[$HO_2C–C_6H_4–SO_3^-$]$_2$) contain the supplementary crystallographic data for this paper. These data can be obtained free of charge via www.ccdc.cam.ac.uk/data_request/cif, or by emailing data_request@ccdc.cam.ac.uk, or by contacting The Cambridge Crystallographic Data Centre, 12 Union Road, Cambridge CB2 1EZ, UK; fax: +44 1223 336033.

AUTHOR INFORMATION

Corresponding authors:

* E-mail: abdelkrim.elghayouri@univ-angers.fr, canadell@icmab.es, and patrick.batail@univ-angers.fr

ORCID

Père Alemany: 0000-0002-3139-6189

Enric Canadell: 0000-0002-4663-5226

Patrick Batail: 0000-0001-7125-5009

CONFLICTS OF INTEREST

The authors declare no conflict of interest.

REFERENCES

1 Wudl, F.; Wobschall, D.; Hufnagel, E.J. Electrical conductivity by the bis(1,3-dithiole)-bis(1,3-dithiolium) system. *J. Am. Chem. Soc.* **1972**, *94*, 670-672.

2 Bendikov, M.; Wudl, F.; Perepichka, D. F. Tetrathiafulvalenes, Oligoacenenes, and Their Buckminsterfullerene Derivatives: The Brick and Mortar of Organic Electronics *Chem. Rev.* **2004**, *104*, 4891-4945.

3 *TTF Chemistry: Fundamentals and Applications of Tetrathiafulvalene,* Yamada, J.-Y.; Sugimoto, T. (Eds.), Springer-Verlag: Berlin-Heidelberg-New York, 2004.

4 Fourmigué, M. ; Batail, P. Activation of Hydrogen- and Halogen-Bonding Interactions in Tetrathiafulvalene-Based Crystalline Molecular Conductors. *Chem. Rev.* **2004**, *104*, 5379-5418.

5 Heuzé, K.; Fourmigué, M.; Batail, P.; Canadell, E.; Auban-Senzier, P. Directing the Structures and Collective Electronic Properties of Organic Conductors: The Interplay of π-Overlap Interactions and Hydrogen Bonds. *Chem. Eur. J.* **1999**, *5*, 2971-2976.

6 Heuzé, K.; Mézière, C. ; Fourmigué, M. ; Batail, P. ; Coulon, C. ; Canadell, E. ; Auban-Senzier, P. ; Jérome, D. An Efficient, Redox-Enhanced Pair of Hydrogen-Bond Tweezers for Chloride Anion Recognition, a Key Synthon in the Construction of a Novel Type of Organic Metal based on the Secondary Amide-Functionalized Ethylenedithiotetrathiafulvalene, β‘‘-(EDT-TTF-CONHMe)$_2$[Cl·H$_2$O] *Chem. Mater.* **2000**, *12*, 1898-1904.

7 Heuzé, K.; Fourmigué, M.; Batail, P.; Coulon, C.; Clérac, R.; Canadell, E.; Auban-Senzier, P.; Ravy, S.; Jérome, D. A Genuine Quarter-Filled Band Mott Insulator, (EDT-TTF-CONMe$_2$)$_2$AsF$_6$: Where the Chemistry and Physics of Weak Intermolecular Interactions Act in Unison *Adv. Mater.* **2003**, *15*, 1251-1254.

8 Kobayashi, Y. Pure Organic Conductors Based on Protonic-Defect Induction: From Semiconductors to Organic Metals *Bull. Chem. Soc. Jpn* **2018**, *91*, 467-485.

9 Dolbecq, A. ; Fourmigué, M. ; Batail, P. ; Coulon, C. From Racemic Mixtures of Chiral □-Donor Molecules to Mixed Stacks of H-Bonded Centrosymmetrical Dimers of Cation and Anion Radicals with Singlet-Triplet Excitations: The Example of [(±)-Me$_3$TTF-C* H(Me)OH$^{\cdot+}$]$_2$[TCNQ$^{\cdot-}$]$_2$ (TTF = Tetrathiafulvalene; TCNQ = Tetracyanoquinodimethane). *Chem. Mater*. **1994**, *6*, 1413-1418.

10 Blanchard, P.; Boubekeur, K.; Sallé, M.; Duguay, G.; Jubault, M.; Gorgues, A.; Martin, J. D.; Canadell, E.; Auban-Senzier, P.; Jérome, D.; Batail, P. A construction principle of the κ-phase

based on the efficient (O-H)donor···Oanion structural functionality: The examples of κ-(EDT–TTF(CH_2OH))$_2$X (X = ClO_4^- and ReO_4^-). *Adv. Mater.* **1992**, *4*, 579-581.

11 Dolbecq, A. ; Guirauden, A. ; Fourmigué, M. ; Boubekeur, K. ; Batail, P. ; Rohmer, M.-M. ; Bénard, M. ; Coulon, C. ; Sallé, M. ; Blanchard, P. Relative basicities of the oxygen atoms of the Linquist polyoxometalate $[Mo_6O_{19}]^{2-}$ and their recognition by hydroxyl groups in radical cation salts based on functionalized tetrathiafulvalene π donors. *J. Chem. Soc., Dalton Trans*. **1999,** 1241-1248.

12 Dolbecq, A. ; Fourmigué, M. ; Krebs, F. C. ; Batail, P. ; Canadell, E. ; Clérac, R. ; Coulon, C. $Me_3TTF–PO_3H_2$, a Redox Phosphonic Acid and Its Monoanilinium Salt $[PhNH^{+3}][Me_3TTF–PO(OH)O^-]$, the Electrocrystallized Neutral (Zwitterionic) π Radical $[Me_3TTF–PO(OH)O^-]^{\cdot+}$, and Their Associated Lamellar Constructions in the Solid State. *Chem. Eur. J.* **1996**, *2*, 1275-1282.

13 Murata, T.; Morita, Y.; Fukui, K.; Sato, K.; Shiomi, D.; Takui, T.; Maesato, M.; Yamochi, H..; Saito, G.; Nakasuji, K. Bonded Charge-Transfer Complex: Crystal Structure and Electronic Properties of TTF-Imidazole–*p*-Chloranil. *Angew. Chem. Int. Ed.* **2004**, *43*, 6343-6346.

14 Brown, R. L.; Brooks, A. C.; Griffiths, J.-P.; Vital, B.; Day, P.; Wallis, J. D. Synthesis of bis(ethylenedithio)tetrathiafulvalene (BEDT-TTF) derivatives functionalised with two, four or eight hydroxyl groups. *Org. Biomol. Chem*. **2007**, *5*, 3172-3182.

15 Batsanov, A. S.; Bryce, M. R.; Cooke, G.; Heaton, J. N.; Howard, J. A. K. 4-(N-Methylthioamido)tetrathiafulvalene: a new kappa-phase structure *J. Chem. Soc., Chem. Commun.* **1993**, 1701-1702.

16 Moore, A. J.; Bryce, M. R.; Batsanov, A. S.; Heaton, J. N.; Lehmann, C. W.; Howard, J. A. K.; Robertson, N.; Underhill, A. E.; Perepichka, I. F. (N-Methylthiocarbamoyl)tetrathiafulvalene derivatives and their radical cations: synthetic and X-ray structural studies. *J. Mater. Chem*. **1998**, *8*, 1541-1550.

17 Murata, T.; Yakiyama, Y.; Nakasuji, K.; Morita Y. Proton-transfer salts between an EDT-TTF derivative having imidazole-ring and anilic acids: multi-dimensional networks by acid-base hydrogen-bonds, π-stacks and chalcogen atom interactions. *CrystEngComm.* **2011**, *13*, 3689-3691.

18 Murata, T.; Nakasuji, K.; Morita, Y. Tetrathiafulvalene-Type Electron Donors Bearing Biimidazole Moieties: Multifunctional Units with Hydrogen Bonding Abilities. *Eur. J. Org. Chem.* **2012**, 4123-4129.

19 Murata, T.; Miyazaki, E.; Maki, S.; Umemoto, Y.; Ohmoto, M.; Nakasuji, K.; Morita, Y. Development of Organic Conductors with Self-Assembled Architectures of Biomolecules:

Synthesis and Crystal Structures of Nucleobase-Functionalized Tetrathiafulvalene Derivatives. *Bull. Chem. Soc. Jpn.* **2012**, *85*, 995-1006.

20 Morita, Y.; Murata, T.; Nakasuji, K. Cooperation of Hydrogen-Bond and Charge-Transfer Interactions in Molecular Complexes in the Solid State. *Bull. Chem. Soc. Jpn.* **2013**, *86*, 183-197.

21 Kamo, H.; Ueda, A.; Isono, T.; Takahashi, K.; Mori, H. Synthesis and properties of catechol-fused tetrathiafulvalene derivatives and their hydrogen-bonded conductive charge-transfer salts. *Tet. Lett*. **2012**, *53*, 4385-4388.

22 Isono, T.; Kamo, H.; Ueda, A.; Takahashi, K.; Nakao, A.; Kumai, R.; Nakao, H.; Kobayashi, K.; Murakami, Y.; Mori, H. Hydrogen bond-promoted metallic state in a purely organic single-component conductor under pressure. *Nature Commun*. **2013**, *4*, 1344.

23 Lakhdar, Y.; Mézière, C.; Zorina, L.; Giffard, M.; Batail, P.; Canadell, E.; Auban-Senzier, P.; Pasquier, C.; Jérome, D.; Nafradi, B.; Forro, L. Dual [proton]/[hole] mixed valence in a molecular metal: balancing chemical activity in the solid state by tapping into a molecular hole reservoir *J. Mater. Chem.* **2011**, *21*, 1516–1522.

24 Lakhdar, Y.; El-Ghayoury, A.; Zorina, L.; Mercier, N.; Allain, M.; Mézière, C.; Auban-Senzier, P.; Batail, P.; Giffard, M. Acentric Polymeric Chains in Radical Cation Salts of Tetrathiafulvalene Derivatives with the *p*-Carboxybenzenesulfonate Anion. *Eur. J. Inorg. Chem.* **2010**, 3338-3342.

25 Whangbo, M.-H.; Williams, J. M.; Leung, P. C. W.; Beno, M. A.; Emge, T. J.; Wang, H.-H. Role of the intermolecular interactions in the two-dimensional ambient-pressure organic superconductors β-$(ET)_2I_3$ and β-$(ET)_2IBr_2$ *Inorg. Chem*., **1985**, *24*, 3500-3502.

26 Williams, J. M.; Wang, H.-H.; Emge, T. J.; Geiser, U.; Beno, M. A.; Leung, P. C. W.; Carlson, K. D.; Thorn, R. J.; Schultz, A. J.; Whangbo, M.-H. Rational Design of Synthetic Metal Superconductors. *Prog. Inorg. Chem*. **1987**, *35*, 51-218.

27 Jung, D.; Evain, M.; Novoa, J. J.; Whangbo, M.-H.; Beno, M. A.; Kini, A. M.; Schultz, A. J.; Williams, J. M.; Nigrey, P. J. Similarities and differences in the structural and electronic properties of κ-phase organic conducting and superconducting salts. *Inorg. Chem*. **1989**, *28*, 4516-4522.

28 Moser, J.; Gabay, M.; Auban-Senzier, P.; Jérome, D.; Bechgaard, K.; Fabre, J. M. Transverse transport in $(TM)_2X$ organic conductors: possible evidence for a Luttinger liquid. *Eur. Phys. J. B*, **1998**, *1*, 39.

29 Ito, H.; Ishiguro, T.; Kubota, M.; Saito, G. Metal-Nonmetal Transition and Superconductivity Localization in the Two-Dimensional Conductor κ-$(BEDT\text{-}TTF)_2Cu[N(CN)_2]Cl$ under Pressure *J. Phys. Soc. Jpn*. **1996**, *65*, 2987-2993.

30 Yasin, S. ; Dumm, M. ; Salameh, B. ; Batail, P. ; Mézière, C. ; Dressel, M. Transport studies at the Mott transition of the two-dimensional organic metal κ-(BEDT-TTF)$_2$Cu[N(CN)$_2$]Br$_x$Cl$_{1-x}$. *Eur. Phys. J. B*, **2011**, *79*, 383-390.

31 El-Ghayoury, A.; Mézière, C.; Simonov, S.; Zorina, L.; Cobián, M.; Canadell, E.; Rovira, C.; Náfrádi, B.; Sipos, B.; Forró, L.; Batail, P. A Neutral Zwitterionic Molecular Solid. *Chem. Eur. J.* **2010**, *16*, 14051-14059.

32 Sheldrick, G. M. A short history of SHELX. *Acta Crystallogr. Sect. A* **2008**, *64*, 112-122.

33 Whangbo, M.-H.; Hoffmann, R. The Band Structure of the Tetracyanoplatinate Chain. *J. Am. Chem. Soc.* **1978**, *100*, 6093–6098.

34 Ammeter, J. H.; Bürgi, H.-B.; Thibeault, J.; Hoffmann, R. Counterintuitive Orbital Mixing in Semiempirical and ab Initio Molecular Orbital Calculations. *J. Am. Chem. Soc.* **1978**, *100*, 3686–3692.

35 Pénicaud, A.; Boubekeur, K.; Batail, P.; Canadell, E.; Auban-Senzier, P.; Jérome, D. Hydrogen-Bond Tuning of Macroscopic Transport Properties from the Neutral Molecular Component Site along the Series of Metallic Organic-Inorganic Solvates (BEDT-TTF)$_4$Re$_6$Se$_5$C1$_9$·[guest], [guest = DMF, THF, dioxane]. *J. Am. Chem. Soc.* **1993**, *115*, 4101–4112.

36 Baudron, S. A.; Avarvari, N.; Canadell, E.; Auban-Senzier, P.; Batail, P. Structural Isomerism in Crystals of Redox-Active Secondary ortho-Diamides: The Role of Competing Intra- and Intermolecular Hydrogen Bonds in Directing Crystalline Topologies *Chem. Eur. J*. **2004**, *10*, 4498-4511.

37 Hohenberg, P.; Kohn, W. Inhomogeneous Electron Gas. *Phys. Rev*., **1965**, *136*, B864–B871. ;

38 Kohn, W.; Sham L. J. Self-Consistent Equations Including Exchange and Correlation Effects. *Phys. Rev.,* **1965**, *140*, A1133–A1138.

39 Soler J. M.; Artacho E.; Gale J. D.; García A.; Junquera J.; Ordejón P.; Sánchez-Portal, D. J. The SIESTA method for ab initio order-N materials simulation. *J. Phys.: Condens. Matter.* **2002**, *14*, 2745–2779.

40 Artacho, E.; Anglada, E.; Diéguez, O.; Gale, J. D.; García, A.; Junquera, J.; Martin, R. M.; Ordejón, P.; Pruneda, J. M.; Sánchez-Portal, D.; Soler J. M. *J.* The SIESTA method: developments and applicability. *Phys.: Condens. Matter*. **2008**, *20*, 064208.

41 For more information on the SIESTA code visit: http://departments.icmab.es/leem/siesta/

42 Perdew, J. P.; Burke, K.; Ernzerhof, M. Generalized Gradient Approximation Made Simple. *Phys. Rev. Lett.* **1966**, *77*, 3865–3868

423 Troullier, N.; Martins J. L. Efficient Pseudopotentials for plane-wave calculations. *Phys. Rev. B* **1991**, 43, 1993–2006.

44 Kleinman, L.; Bylander, D. M. Efficacious Form for Model Pseudopotentials. *Phys. Rev. Lett.* **1982**, 48, 1425–1428.

45 Artacho, E.; Sánchez-Portal, D.; Ordejón, P.; García, A.; Soler, J. M. Linear Scaling ab-initio Calculations for Large and Complex Systems. *Phys. Stat. Sol. (b)* **1999**, *215*, 809–817.

46 Kiyota, Y.; Jeon, I.-E.; Jeannin, O.; Beau, M.; Kawamoto, T.; Alemany, P.; Canadell, E.; Mori, T.; Fourmigué, M. Electronic engineering of a tetrathiafulvalene charge-transfer salt via reduced symmetry induced by combined substituents. *Phys. Chem. Chem. Phys*. **2019**, *21*, 22639-22646.

47 Dudarev, S. L.; Botton, G. A.; Savrasov, S. Y.; Humphreys, C. J.; Sutton, A. P. Electron-energy-loss spectra and the structural stability of nickel oxide: An LSDA+U study *Phys. Rev. B*, **1998**, *57*, 1505-1509.

48 Monkhorst, H. J.; Pack J. D. Special points for Brillouin zone integrations. *Phys. Rev. B* **1976**, *13*, 5188–5192.

Graphical Abstract